Research Square

Preprints are preliminary reports that have not undergone peer review.
They should not be considered conclusive, used to inform clinical practice,
or referenced by the media as validated information.

Three permissiveness gates multiply to determine mutation realisation: age-specific incidence and the dialysis–transplant separation from one parameter set

qiaoxuan wei

358679132@qq.com

The Fourth People's Hospital of Nanning https://orcid.org/0009-0003-7824-0311

yu-ting ma

The Fourth People's Hospital of Nanning https://orcid.org/0009-0006-8968-0111

gui-juan zhu

The Fourth People's Hospital of Nanning https://orcid.org/0009-0000-2302-9912

Research Article

Keywords: Tumour permissive mutation, three gates, product model, age-specific incidence, dialysis–transplant separation, pre-malignant screening

Posted Date: November 3rd, 2026

DOI: https://doi.org/10.21203/rs.3.rs-11544766/v1

License: This work is licensed under a Creative Commons Attribution 4.0 International License.
Read Full License

Additional Declarations: The authors declare no competing interests.

Abstract

Background

Mutation realisation is set by the product of three permissiveness gates: intrinsic G1, tissue G2 and systemic G3. An expanded clone appears only when all three are non-zero. Age-specific incidence and the dialysis–transplant separation are two readouts of the same product.

Methods

We analysed published data. SEER 2010–2013 supplied the multistage-senescence parameters k and b for 20 non-reproductive cancers. ANZDATA supplied cancer SMRs for 52,936 dialysis patients and 16,820 transplant recipients. Driver-mutation clones in normal colon and oesophagus constrained G1. We estimated k, b and G2, compared the three-gate product with one-gate, two-gate and additive models, and tested the result against HALO-301 and the anti-CD47 phase III trial.

Results

k = 6.17, b = 0.0099 ± 0.0005 yr^{-1}, non-driver rate-limiting steps 4.43 (72%). Dialysis SMR 1.2, transplant SMR 2.6, ratio r = 2.17; with transplant set to 1, dialysis G2 = 0.46. Peak age about 85 years, matching the fitted SEER plateau. The product reproduces both the inverted-U incidence curve and the dialysis–transplant separation. The one-gate and two-gate models satisfy one of the two. The additive model returns output when a gate is zero. Both interventions improved technical endpoints without changing overall survival.

Conclusions

Permissiveness is a product gate. G2 sets the amplitude of incidence; G1 and G3 set the shape of the age curve. Screening and treatment are directed at the lowest gate.

1 Introduction

Mutation realisation is controlled by three permissiveness gates, and age-specific incidence is the readout of all three acting together. Cancer incidence rises with age, peaks at 80–90 years and then falls.1–3 The multistage-senescence model describes this curve with a stage number k and a senescence-suppression factor b: incidence rises as a power of age and is compressed by a senescence term (1 − bt), so k and b jointly set the peak age.1 That model explains the shape of the curve. It does not answer the next question: why does the same burden of driver mutations produce widely different realisation rates across tissues, immune states and organ function?

The dialysis–transplant contrast turns tissue permissiveness into a number. ANZDATA enrolled 52,936 dialysis patients and 16,820 transplant recipients; after excluding prior cancer, the SMR for incident cancer was 1.2 during dialysis and 2.6 after transplantation.4 Both groups share a baseline of renal impairment, and the difference concentrates in immunosuppression. Cancers that rise consistently after transplantation cluster in virus-related and immune-controlled types; long-latency solid tumours do not appear on that list.5 The separation shows that mutation supply is not the only determinant: the tissue decides whether a clone is let through.

Normal-tissue sequencing pins intrinsic permissiveness at the other end. Driver mutations in KRAS and TP53 are present in normal colonic mucosa, mostly as independent clones.6 TP53-mutant clones accumulate with age in normal oesophagus but remain constrained by clonal competition; p53 mutation alone does not initiate a tumour.7 The multistage-senescence model gives a mean k of 6.17 across 20 non-reproductive cancers. Driver gene counts average 1.74 (Iranzo) or 1.78 (Bailey); non-driver rate-limiting steps are 4.43 or 4.39, 72% of the total.1 Even if every driver mutation were present at birth, 28% of rate-limiting steps would remain. The model assigns the remaining 72% to non-driver stages and does not allocate them across gates.

Four frameworks each explain one factor. Somatic mutation theory explains mutation supply.8 Clonal evolution explains selection within G1.9 The multistage-senescence model explains the G1 × G3 age curve and contains no G2.1 Immunoediting and tissue organisation theory explain how tissue selects clones.8,10 None writes the three as a product. Age-specific incidence and the dialysis–transplant separation therefore sit in two separate accounts, never produced by one parameter set.

We write the three gates as three estimable permissiveness variables: G1(t) for intrinsic, G2 for tissue and G3(t) for systemic permissiveness. The three-gate product model is:

$\lambda(t, G2) = \lambda 0 \times G1(t) \times G2 \times G3(t)$.

The model has four parameters: k, b, G2 and the scale λ0. k and b come from SEER, G2 from the ANZDATA SMR ratio, and λ0 is fixed by incidence at the reference age. We test three things with the same parameter set: whether the model reproduces the inverted U of age-specific incidence; whether it reproduces the 2.17-fold dialysis–transplant separation; and whether it accounts for single-gate intervention that improves technical endpoints without changing clinical endpoints.

2 Methods

2.1 Data sources

We used four published data sources (Table 1). First, the per-cancer parameters of the SEER 2010–2013 multistage-senescence model: stage number k, senescence-suppression factor b and peak age.1 Second, overall and site-specific cancer SMRs from the ANZDATA dialysis and transplant cohorts,4,5 and lung-cancer risk by dialysis vintage and after transplantation.11 Third, driver-mutation clones in normal

colon and normal oesophagus6,7 and two independent driver-gene counts.1 Fourth, intervention controls: the PEGPH20 phase III trial HALO-301,12 and the anti-CD47 phase III trial,13 which we use as external samples of single-gate intervention.

Table 1 Data sources and their roles

Source	Content	Role in this study
SEER 2010–2013 multistage-senescence model1	k, b, peak age and driver gene counts for 20 non-reproductive cancers	Estimate the stage term of G1 and the senescence term of G3
ANZDATA dialysis and transplant cohorts4	52,936 dialysis patients and 16,820 transplant recipients; incident cancer SMR	Estimate G2
ANZDATA site-specific analysis5	Cancers that rise after dialysis and after transplantation	Test the tissue specificity of G2
Normal colon and oesophagus sequencing6,7	KRAS, TP53 and other driver-mutation clones	Constrain mutation supply in G1
HALO-301 12	PEGPH20 phase III; ORR, OS, PFS, DOR	External sample of single-gate intervention
Anti-CD47 studies and phase III13-16	CD47 cis masking, regulation and trial termination	External sample of single-gate intervention

2.2 The three-gate product model

Let t be age, G1(t) intrinsic permissiveness, G2 tissue permissiveness and G3(t) systemic permissiveness. Each takes values from 0 to 1; 0 is a closed gate and 1 a fully open gate. The model is:

$\lambda(t, G2) = \lambda_0 \times G1(t) \times G2 \times G3(t)$.

The three terms are defined as follows.

G1(t) = (t/50)^(k−1), normalised to 1 at age 50. The exponent is k−1, matching ASR(t) = a × t^(k−1) × (1 − bt) in the source model.1

G3(t) = (1 − bt)/(1 − 50b), normalised to 1 at age 50. The domain is $50 \le t \le 1/b$; beyond 1/b the senescence term turns negative and the model does not apply.

G2 is 1 for transplant and 1/r for dialysis, where r = SMR(transplant)/SMR(dialysis).

λ_0 is the scale at age 50 with G2 = 1, fixed by incidence at the reference age. k and b come from SEER, G2 from ANZDATA; λ_0 is a scale, not a free fitted parameter.

When G1, G2 and G3 take only 0 or 1, the product collapses to a Boolean AND gate: $\lambda = \lambda_0$ when all three are 1, and $\lambda = 0$ when any is 0. The truth table is the 0/1 limit of the product model (Table 5). “All three required” and “continuous permissiveness” are two scales of one model.

The model rests on three assumptions. First, G1 is a stage-accumulation term; k summarises intrinsic mechanisms and does not measure apoptosis or senescence directly. Second, G2 is a tissue multiplier that does not change with age; if tissue permissiveness were age-dependent, the model would need G2(t). Third, G3 is a senescence-execution term summarised by b; it does not separate organ function, inflammation and metabolism as distinct sources.

2.3 Parameter estimation

We take k and b from the pooled values for 20 non-reproductive cancers: $k = 6.17$ and $b = 0.0099 \pm 0.0005\ yr^{-1}$.1 Non-driver rate-limiting steps = k − driver gene count = 4.43 (Iranzo) or 4.39 (Bailey), 72% of the total.1

We estimate G2 from the ANZDATA SMR ratio: $r = 2.6/1.2 = 2.17$, G2(transplant) = 1.00 and G2(dialysis) = 1/2.17 = 0.46. The parameter is calibrated directly from observed values, not fitted. The model then predicts a transplant-to-dialysis incidence ratio of 2.17. That prediction is a consistency check, not independent validation. We compare normalised curves and ratios rather than absolute incidence; λ_0 serves only to align scale.

The fitted form $T_p = k/[b(k+1)]$ gives a peak near 85 years for non-reproductive cancers.1 The mathematical peak of the average-parameter curve, $(k-1)/(bk) = 84.6$ years, differs from the fitted plateau by 0.4 years.

2.4 Model comparison

We compare four models:

1. One-gate: $\lambda = \lambda_0 \times G1(t)$.
2. Two-gate: $\lambda = \lambda_0 \times G1(t) \times G3(t)$.
3. Additive: $\lambda = \lambda_0 \times (G1 + G2 + G3)$.
4. Three-gate product: $\lambda = \lambda_0 \times G1 \times G2 \times G3$.

We apply three criteria: whether the model reproduces the inverted U of age-specific incidence; whether it reproduces the 2.17-fold dialysis–transplant separation; and whether output falls to zero when any gate is zero. We retain a model that meets all three and reject one that misses any. This is a structural comparison. All four models share k and b, and we compare whether they produce the two phenomena rather than AIC or likelihood ratios. Registry data carry no individual-level gate measurements, so a goodness-of-fit comparison requires a prospective cohort.

2.5 Evidence grading

We grade the evidence at three levels. Direct evidence: the SEER k and b and the ANZDATA SMRs, which are published measurements or model parameters. Concordant evidence: the site-specific cancer list, normal-tissue mutation clones, and the direction of the intervention controls. Model inference: the functional forms of G1 and G3, the product structure, and the allocation of 4.43 steps across gates.

2.6 Ethics and data

The analysis uses public data and published literature. Table 2 carries every parameter needed to recompute it.

3 Results

3.1 Gate 1: intrinsic permissiveness G1

Two lines of evidence constrain intrinsic permissiveness. First, driver mutations are already present in normal tissue. Normal colonic mucosa carries KRAS and TP53 driver mutations, mostly as independent clones.6 TP53-mutant clones accumulate with age in normal oesophagus but remain constrained by clonal competition; p53 mutation alone does not initiate a tumour.7 Second, the rate-limiting-step account: across 20 non-reproductive cancers the mean k is 6.17, driver gene counts average 1.74 or 1.78, and non-driver rate-limiting steps are 4.43 or 4.39, 72% of the total.1

Driver-mutant clones persist in normal tissue, so the G1 bottleneck lies in whether each stage becomes rate-limiting, not in mutation supply. Clonal competition constrains p53-mutant clones in normal oesophagus, and a single mutation does not initiate a tumour.7 G1 is multistep. The same model reports that men have about 14% more stages and a 33% higher stage-transition rate than women;1 G1 accommodates the sex difference without a separate gate.

The three-gate model requires at least one rate-limiting step per gate. Three gates need at least three non-driver steps, and the observed 4.43 meets that floor. 4.43 cannot be assigned uniquely to G1, G2 and G3, and it does not distinguish three gates from four or five. The gate number is a model setting; the data constrain the total, not the number of gates. Three gates are the smallest structure that satisfies the floor.

G1(t) takes the multistage accumulation term, G1(t) = (t/50)^(k−1), normalised to 1 at age 50. With k = 6.17, Table 3 gives G1 at 60, 70, 80, 85, 90 and 95 years. G1 rises monotonically with age and cannot by itself produce the decline at the oldest ages. Intrinsic mechanisms include replication stress, apoptosis, senescence, ROS and ferroptosis;17-19 k summarises them in this model.

3.2 Gate 2: tissue permissiveness G2

ANZDATA enrolled 52,936 dialysis patients and 16,820 transplant recipients. After excluding prior cancer, the SMR for incident cancer was 1.2 during dialysis and 2.6 after transplantation.4 Both groups share a baseline of renal impairment, and the difference concentrates in immunosuppression intensity. Cancers that rise after transplantation cluster in virus-related and immune-controlled types; long-latency solid tumours do not rise in parallel.5 Cancer risk after transplantation increases linearly with time on dialysis (Ptrend = 0.02), and the risk of lung cancer is highest in recipients with the longest dialysis vintage (aHR 3.32, 95% CI 1.00-11.4).11 Oxidative DNA damage increases during dialysis;20,21 that gives concordant evidence for G1 substrate accumulating while G2 stays closed.

G2 is calibrated from the SMR ratio: r = 2.6/1.2 = 2.17, G2(transplant) = 1.00 and G2(dialysis) = 0.46. The model predicts a transplant-to-dialysis incidence ratio of 2.17, which matches the observed value. That agreement follows from calibration; the independent information lies in the site-specific pattern. Tissue permissiveness should vary by tissue rather than scale every cancer equally.

The site-specific pattern constrains the model further. Across the two immunosuppressed cohorts, the cancers that rise consistently are NMSC, non-Hodgkin lymphoma, and cancer of the lip, kidney, larynx and thyroid. Long-latency solid tumours — lung, breast, colorectal, gastric, prostate, pancreatic and ovarian — do not appear on that list.5 A single multiplier shared by all cancers would scale every type equally; in the data, virus-related and immune-controlled cancers rise first. The site-specific pattern shows that G2 varies by tissue. The present model uses one average G2 for all cancers and does not capture this heterogeneity; systemic immunosuppression accounts for part of it.

Tissue permissiveness draws on antigen presentation, NK/CD8 killing, Treg/MDSC suppression, CAF/ECM barriers, normal stem-cell competition, perfusion and lymphatic drainage.10,22,23 Environmental normalisation experiments support its manipulability. Teratocarcinoma nuclei participate in normal development in a normal embryonic environment.24 Transformed liver epithelial cells regress after transplantation back into liver.25 Young mammary stroma normalises mammary tumour cells; old stroma does not.26 The embryonic neural-crest microenvironment reprograms multipotent tumour cells.27 The same cells change fate when only the environment changes. Clones stay silent in tissue for years until the systemic window opens;28 that is G2 held low while G3 is not yet open.

3.3 Gate 3: systemic permissiveness G3

G3(t) takes the senescence-execution term, G3(t) = (1 − bt)/(1 − 50b), normalised to 1 at age 50, with b = 0.0099 ± 0.0005 yr^{-1}.1 Table 3 gives G3 at 60, 70, 80, 85, 90 and 95 years. G3 falls with age; on its own it cannot produce the inverted U, because G1 rises monotonically, G3 falls monotonically, and their product peaks in between.

b is nearly constant across 20 non-reproductive cancers with different aetiologies; 1/b is about 101 years.1 We attribute this constancy to a shared G3 decay term that crosses cancer types. In the model,

the post-peak decline comes from the G3 execution term: at the same mutation burden, lower organ function and metabolic execution give a lower realisation rate.

The fitted peak is about 85 years;1 the mathematical peak of the average-parameter curve is 84.6 years, 0.4 years below the fitted plateau. The decline at the oldest ages comes from the G3 execution term: mutation supply keeps rising with age while realisation falls with execution capacity.

Systemic permissiveness includes organ function, systemic inflammation, substrate and energy, neuroendocrine state, circadian rhythm and acute events. The postoperative window is an acute version of G3: in animal models, surgery awakens distant dormant tumours;29 extracellular vesicles from early lung cancer carry increased CD47.30 G3 is a systemic state that moves with organ function, inflammation and acute events, not with age alone.

3.4 The three-gate product

Multiplying the three terms gives $\lambda(t, G2) = \lambda 0 \times G1(t) \times G2 \times G3(t)$.

Normalised to age 50, G1 × G3 takes the values 2.06, 3.46, 4.68, 4.88, 4.51 and 3.25 at 60, 70, 80, 85, 90 and 95 years (Table 3, Figure 1). The product peaks at 85 years and then falls. The inverted U comes from the opposing directions of G1 and G3; no additional old-age suppression parameter is needed.

G2 changes amplitude, not shape. In the product model G2 is a multiplier, so the dialysis and transplant age curves have the same shape and differ only by scale. The prediction is directly testable: if the two curves differ in shape, G2 must be written as G2(t) and the model needs a tissue-specific time term. We have no individual age-specific transplant cancer data.

Sensitivity analysis gives the parameter range. With k between 5.9 and 6.5 and b between 0.0095 and 0.0103 yr^{-1}, the mathematical peak of the average-parameter curve falls between 80.6 and 89.1 years. With SMRs between 1.1 and 1.3 for dialysis and between 2.4 and 2.8 for transplant, r falls between 1.85 and 2.55 and G2(dialysis) between 0.39 and 0.54. Peak position and the direction of the twofold separation do not change.

At the 0/1 limit the product becomes an AND gate (Table 5): only 1-1-1 gives output 1, and the other seven rows give 0.

3.5 Model comparison and external samples

Table 4 compares the four models. The one-gate model has only G1; its age curve rises monotonically and shows no decline at the oldest ages; rejected. The two-gate model G1 × G3 produces the inverted U but not the dialysis–transplant separation; rejected. The additive model G1 + G2 + G3 produces both the inverted U and the separation; it still returns non-zero output when a gate is zero, so it fails the boundary

condition; rejected. The three-gate product meets all three criteria — inverted U, 2.17-fold separation, zero output at a zero gate; retained.

Two trials provide external samples of single-gate intervention. In HALO-301, PEGPH20 raised the objective response rate from 36% to 47%. Median overall survival was 11.2 versus 11.5 months, median progression-free survival 7.1 versus 7.1 months, and duration of response did not improve. Toxicity increased: fatigue 16.0% versus 9.6%, muscle spasm 6.5% versus 0.6%, and hyponatraemia 8.0% versus 3.8%.12 CD47 masks pro-phagocytic ligands in cis and forms a ratio with eat-me ligands;14 pro-inflammatory signalling reaches CD47 through a super-enhancer;15 and HIF-1 regulates CD47.16 Natural products have acted on the CD47 axis in three experimental models.31-33 The anti-CD47 phase III trial was terminated.13 Each intervention hits one link: matrix breakdown or the don't-eat-me signal. In the product model the effect of a single-gate intervention is scaled by the product of the other two gates; when those two are limiting, a single-link improvement does not change total output. Response rate reads one link; overall survival reads the product. The separation between them follows.

Table 2 Parameters of the three-gate model

Parameter	Meaning	Estimate	Source and method
k	Number of rate-limiting stages	6.17	SEER multistage-senescence model1
b	Senescence-suppression factor	0.0099 ± 0.0005 yr^{-1}	SEER fit1
Driver genes	Number of driver mutations	1.74 (Iranzo) / 1.78 (Bailey)	Literature count1
Non-driver steps	k — driver genes	4.43 / 4.39 (72%)	Calculated1
r	Tissue permissiveness ratio	2.17	SMR 2.6/1.24
G2 (dialysis)	Dialysis tissue permissiveness	0.46	1/r, normalised
G2 (transplant)	Transplant tissue permissiveness	1.00	Normalised
Tp	Peak age	85 years	SEER per-cancer fit1

Table 3 Normalised permissiveness predicted by the model

Age (years)	G1	G3	G1 × G3
50	1.00	1.00	1.00
60	2.57	0.804	2.06
70	5.69	0.608	3.46
80	11.36	0.412	4.68
85	15.54	0.314	4.88
90	20.88	0.216	4.51
95	27.62	0.118	3.25

Table 4 Comparison of four models

Model	Inverted U	Dialysis-transplant separation	Zero output at a zero gate	Verdict
One-gate G1	No	No	Cannot express: no G2 or G3	Rejected
Two-gate G1 × G3	Yes	No	Cannot express: no G2	Rejected
Additive G1 + G2 + G3	Yes	Yes	No	Rejected
Three-gate product G1 × G2 × G3	Yes	Yes	Yes	Retained

Table 5 Boolean limit of the three-gate product model

G1	G2	G3	λ
0	0	0	0
1	0	0	0
1	1	0	0
1	1	1	λ0
1	0	1	0
0	1	1	0
0	0	1	0
0	1	0	0

4 Discussion

4.1 Main findings

We write three-gate permissiveness as a four-parameter product model: $\lambda = \lambda_0 \times G1 \times G2 \times G3$, with k = 6.17, b = 0.0099, G2 ratio = 2.17 and Tp = 85 years. The model reproduces both the inverted-U age curve and the dialysis–transplant separation. The one-gate and two-gate models satisfy one of the two, and the additive model fails the zero-gate boundary. At the 0/1 limit the product becomes an AND gate.

4.2 Mechanisms of the three gates

G1 is intrinsic self-limitation: replication stress, apoptosis, senescence, ROS and ferroptosis.17–19 Driver mutations are already present in normal tissue, and most clones are held by these programmes.6,7 G1 decides whether a mutant cell bypasses them; it does not decide whether mutation exists.

G2 is tissue constraint: antigen presentation, NK/CD8 killing, Treg/MDSC suppression, CAF/ECM barriers, normal stem-cell competition, perfusion and lymphatic drainage.10,22,23 Environmental normalisation experiments show that the same cells change fate when the environment changes.24–27 Transplantation immunosuppression raises G2: with transplant set to 1.00 and dialysis to 0.46, the transplant group has 2.17 times the cancer SMR of the dialysis group.4,5

G3 is systemic permissiveness: organ function, systemic inflammation, substrate and energy, neuroendocrine state, circadian rhythm and acute events. We read b as the projection of G3 onto the age axis;1 the postoperative window is an acute version of G3.29,30 G3 falls through execution capacity while mutation supply keeps rising.

The three gates multiply in either order, and each has its own site: G1 inside the cell, G2 at the tissue interface, and G3 at the level of the whole organism. A clone is realised when all three are non-zero within the same time window. The product describes the condition for realisation, not the order of events; order requires individual longitudinal data.

4.3 Four frameworks each explain one factor, the product explains two phenomena

Somatic mutation theory explains mutation supply.8 Clonal evolution explains selection within G1.9 The multistage-senescence model explains the G1 × G3 age curve and contains no G2.1 Immunoediting and tissue organisation theory explain how tissue selects clones.8,10 Each explains one factor; none writes the three as a product. The three-gate model places all four in one product.

The difference from the additive model is the boundary. The additive model returns output when a gate is zero; the product returns zero. HALO-301 and the anti-CD47 trial match the product: single-gate endpoints improve and overall survival does not, which shows that the other two gates were still limiting.12,13

The three-gate product is isomorphic to the multistage-senescence model. That model's ASR = a × t^(k − 1) × (1 − bt) is the unnormalised form of G1(t) × G3(t); the three-gate model extends it to three factors and adds the tissue term G2.

The model makes four testable predictions. First, the dialysis and transplant age-specific incidence curves have the same shape and differ only by scale; a difference in shape would mean that G2 is not a single multiplier. Second, a G2 intervention changes amplitude but not peak age, while a G1 or G3 intervention changes peak age. Third, the effect of a single-gate intervention on overall survival depends on the other two gates; when those are limiting, the effect approaches zero. Fourth, in independent cohorts, tissues with higher G2 show higher SMRs for virus-related and immune-controlled cancers, and long-latency solid tumours have lower G2.

4.4 Clinical implications

A G2 intervention changes amplitude, not the shape of the age curve. Immune restoration, stromal reset and perfusion reconstruction belong to G2; they lower post-transplant cancer incidence without shifting the peak age. A G1 intervention changes the rising limb; a G3 intervention changes the decline at the oldest ages.

Pre-malignant screening has three levels. The G1 level reads driver-mutant clones in normal tissue and intrinsic execution markers;6,7 the G2 level reads immune composition, ECM and perfusion; the G3 level reads organ function, inflammation and metabolism. The three levels read together identify which gate an individual is missing. A single level reports the state of one gate and does not give the product.

Treatment is directed by gate. The model's criterion is that the lowest gate sets where the intervention goes. The effect of an intervention elsewhere is scaled by the value of that lowest gate, which matches the rise in response rate without a change in overall survival in HALO-301.

A herbal compound formula carries multiple components and can cover all three gates, unlike a single-target drug that covers one. Coverage is not the product: a formula must first establish which gate each component acts on, and only then address combination. Adding three groups of herbs together returns the additive model.

4.5 The boundaries of the model follow from the data level

G1 summarises the stage number k and does not separate the contributions of apoptosis, senescence, ROS and ferroptosis; the model merges them into one rate-limiting-step count. G2 is calibrated from an SMR ratio, and SMR is a cancer-mortality endpoint; the interpretation of G2 is therefore limited to the tissue permissiveness that corresponds to cancer mortality. Calibration assumes that the dialysis and transplant groups share G1 and G3 at the same age; differences in comorbidity, dialysis vintage and immunosuppressive regimen enter the estimate of G2.

Data level sets the time resolution. SEER and ANZDATA are population registries, and the model's time window is at population level; an individual-level window requires a prospective cohort. The functional

forms of G1 and G3 are model settings; k and b vary with the model family, and another multistage model would give different parameter values. The 4.43 non-driver steps give a lower bound on the total, not an allocation across gates and not a gate count.

The order of G2 and G3 is not identifiable; the model requires only that both are non-zero within the same time window, and registry data cannot determine which comes first.

5 Conclusions

Permissiveness is a product gate: G1, G2 and G3 must all hold for a mutation to be realised as an expanded clone, and a zero at any gate gives zero output. The four parameters — k = 6.17, b = 0.0099, G2 ratio = 2.17 and Tp = 85 years — come from public data and can be recomputed from Table 2. G2 sets the amplitude of incidence; G1 and G3 set the shape of the age curve. Pre-malignant screening and treatment are directed by gate: identify which gate an individual is missing, then restore that gate. Killing clones locally changes one term; the other two still limit total output.

Declarations

Author contributions

Qiao-Xuan Wei designed the study, built the model, analysed the data and wrote the first draft. Yu-Ting Ma contributed clinical interpretation, literature verification and revision. Gui-Juan Zhu checked the data and tables and revised the manuscript. All authors read and approved the final manuscript.

Competing interests

We declare no competing interests.

Funding

This work received no specific funding from any public, commercial or non-profit agency.

Ethics approval

This is a secondary analysis and theoretical modelling study. It required no new ethics approval.

Data availability

The model parameters and computed tables are in Tables 2 and 3; the sensitivity analysis can be recomputed from Table 2.

References

1. Richardson RB, Anghel CV, Deng DS (2021) Profound synchrony of age-specific incidence rates and tumor suppression for different cancer types as revealed by the multistage-senescence model of carcinogenesis. Aging. ;13(20):23545–23578. 10.18632/aging.203651. PMID: 34695806
2. Tanskanen T, Seppa KJM, Virtanen A et al (2021) Cancer incidence and mortality in the oldest old: a nationwide study in Finland. Am J Epidemiol. ;190(5):836–842. 10.1093/aje/kwaa236. PMID: 33089310
3. Nolen SC, Evans MA, Fischer A et al (2017) Cancer incidence, prevalence and mortality in the oldest-old: a comprehensive review. Mech Ageing Dev. ;164:113–126. 10.1016/j.mad.2017.05.002. PMID: 28502820
4. Au EH, Chapman JR, Craig JC et al (2019) Overall and site-specific cancer mortality in patients on dialysis and after kidney transplant. J Am Soc Nephrol. ;30(3):471–480. 10.1681/ASN.2018090906. PMID: 30765426
5. Hortlund M, Arroyo Muhr LS, Storm H et al (2017) Cancer risks after solid organ transplantation and after long-term dialysis. Int J Cancer. ;140(5):1091–1101. 10.1002/ijc.30531. PMID: 27870055
6. Matas J, Kohrn B, Fredrickson J et al (2022) Colorectal cancer is associated with the presence of cancer driver mutations in normal colon. Cancer Res. ;82(8):1492–1502. 10.1158/0008-5472.CAN-21-3607. PMID: 35425963
7. Murai K, Dentro S, Ong SH et al (2022) p53 mutation in normal esophagus promotes multiple stages of carcinogenesis but is constrained by clonal competition. Nat Commun. ;13(1):6206. 10.1038/s41467-022-33945-y. PMID: 36266286
8. Soto AM, Sonnenschein C (2004) The somatic mutation theory of cancer: growing problems with the paradigm? Bioessays. ;26(10):1097–1107. 10.1002/bies.20087. PMID: 15382143
9. Vendramin R, Litchfield K, Swanton C (2021) Cancer evolution: Darwin and beyond. EMBO J. ;40(18):e108389. 10.15252/embj.2021108389. PMID: 34459009
10. Schreiber RD, Old LJ, Smyth MJ (2011) Cancer immunoediting: integrating immunity's roles in cancer suppression and promotion. Science. ;331(6024):1565–1570. 10.1126/science.1203486. PMID: 21436444
11. Wong G, Turner RM, Chapman JR et al (2013) Time on dialysis and cancer risk after kidney transplantation. Transplantation. ;95(1):114–121. 10.1097/TP.0b013e31827743b4. PMID: 23222892
12. Van Cutsem E, Tempero MA, Sigal D et al (2020) Randomized phase III trial of pegvorhyaluronidase alfa with nab-paclitaxel plus gemcitabine for patients with hyaluronan-high metastatic pancreatic adenocarcinoma. J Clin Oncol. ;38(27):3185–3194. 10.1200/JCO.20.00590. PMID: 32706635
13. Daver N, Vyas P, Huls G et al (2025) The ENHANCE-3 study: venetoclax and azacitidine plus magrolimab or placebo for untreated AML unfit for intensive therapy. Blood. ;146(5):601–611. 10.1182/blood.2024027506. PMID: 40233321

14. Tang Z, Zhong MC, Qian J et al (2023) CD47 masks pro-phagocytic ligands in cis on tumor cells to suppress antitumor immunity. Nat Immunol. ;24(12):2032–2041. 10.1038/s41590-023-01671-2. PMID: 37945822
15. Betancur PA, Abraham BJ, Yiu YY et al (2017) A CD47-associated super-enhancer links pro-inflammatory signalling to CD47 upregulation in breast cancer. Nat Commun. ;8:14802. 10.1038/ncomms14802. PMID: 28378740
16. Zhang H, Lu H, Xiang L et al (2015) HIF-1 regulates CD47 expression in breast cancer cells to promote evasion of phagocytosis and maintenance of cancer stem cells. Proc Natl Acad Sci U S A. ;112(45):E6215-E6223. 10.1073/pnas.1520032112. PMID: 26512116
17. Zhu H, Blake S, Kusuma FK et al (2020) Oncogene-induced senescence: from biology to therapy. Mech Ageing Dev. ;187:111229. 10.1016/j.mad.2020.111229. PMID: 32171687
18. Forcina GC, Dixon SJ (2019) GPX4 at the crossroads of lipid homeostasis and ferroptosis. Proteomics. ;19(18):e1800311. 10.1002/pmic.201800311. PMID: 30888116
19. Hanahan D, Weinberg RA (2011) Hallmarks of cancer: the next generation. Cell. ;144(5):646–674. 10.1016/j.cell.2011.02.013. PMID: 21376230
20. Oberacker T, Fritz P, Schanz M et al (2022) Enhanced oxidative DNA damage in peritoneal dialysis patients via the TXNIP/TRX axis. Antioxidants (Basel). ;11(6):1124. 10.3390/antiox11061124. PMID: 35740021
21. Nemmar A, Karaca T, Beegam S et al (2017) Lung oxidative stress, DNA damage, apoptosis, and fibrosis in adenine-induced chronic kidney disease in mice. Front Physiol. ;8:896. 10.3389/fphys.2017.00896. PMID: 29218013
22. Bejarano L, Jordao MJC, Joyce JA (2021) Therapeutic targeting of the tumor microenvironment. Cancer Discov. ;11(4):933–959. 10.1158/2159-8290.CD-20-1808. PMID: 33811125
23. Kalluri R (2016) The biology and function of fibroblasts in cancer. Nat Rev Cancer. ;16(9):582–598. 10.1038/nrc.2016.73. PMID: 27550820
24. Mintz B, Illmensee K (1975) Normal genetically mosaic mice produced from malignant teratocarcinoma cells. Proc Natl Acad Sci U S A. ;72(9):3585–3589. 10.1073/pnas.72.9.3585. PMID: 1059147
25. McCullough KD, Coleman WB, Smith GJ et al (1997) Age-dependent induction of hepatic tumor regression by the tissue microenvironment after transplantation of neoplastically transformed rat liver epithelial cells into the liver. Cancer Res 57(9):1807–1813 PMID: 9135026
26. Maffini MV, Calabro JM, Soto AM et al (2005) Stromal regulation of neoplastic development: age-dependent normalization of neoplastic mammary cells by mammary stroma. Am J Pathol. ;167(5):1405–1410. 10.1016/S0002-9440(10)61227-8. PMID: 16251424
27. Kasemeier-Kulesa JC, Teddy JM, Postovit LM et al (2008) Reprogramming multipotent tumor cells with the embryonic neural crest microenvironment. Dev Dyn. ;237(10):2657–2666. 10.1002/dvdy.21613. PMID: 18629870

28. Sosa MS, Bragado P, Aguirre-Ghiso JA (2014) Mechanisms of disseminated cancer cell dormancy: an awakening field. Nat Rev Cancer. ;14(9):611–622. 10.1038/nrc3793. PMID: 25118602
29. Krall JA, Reinhardt F, Mercury OA et al (2018) The systemic response to surgery triggers the outgrowth of distant immune-controlled tumors in mouse models of dormancy. Sci Transl Med. ;10(436):eaan3464. 10.1126/scitranslmed.aan3464. PMID: 29643230
30. Chuang CH, Zhen YY, Ma JY et al (2024) CD47-mediated immune evasion in early-stage lung cancer progression. Biochem Biophys Res Commun. ;720:150066. 10.1016/j.bbrc.2024.150066. PMID: 38749193
31. Dai S, Liu Y, Zhao F et al (2022) Aqueous extract of Taxus chinensis var. mairei targeting CD47 enhanced antitumor effects in non-small cell lung cancer. Biomed Pharmacother. ;154:113628. 10.1016/j.biopha.2022.113628. PMID: 36058145
32. Li Z, Gu X, Rao D et al (2021) Luteolin promotes macrophage-mediated phagocytosis by inhibiting CD47 pyroglutamation. Transl Oncol. ;14(8):101129. 10.1016/j.tranon.2021.101129. PMID: 34051623
33. Feng C, Chen R, Fang W et al (2023) Synergistic effect of CD47 blockade in combination with cordycepin treatment against cancer. Front Pharmacol. ;14:1144330. 10.3389/fphar.2023.1144330. PMID: 37138855

Figures

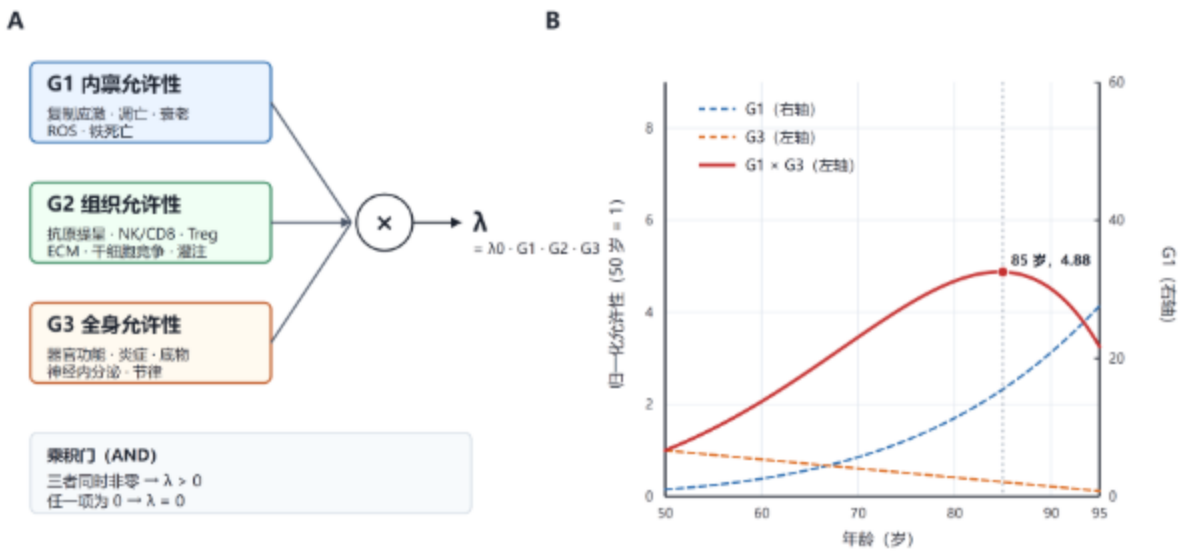


Figure 1

Structure and age curves of the three-gate product model

A: the three gates converge on a product node. B: normalised age curves of G1, G3 and G1 × G3; the product peaks at 85 years.